Topological superconductivity in Rashba semiconductors without a Zeeman field

Panagiotis Kotetes*
Institut für Theoretische Festkörperphysik and DFG-Center for Functional Nanostructures (CFN), Karlsruhe Institute of Technology, 76128 Karlsruhe, Germany

In this manuscript I present new hybrid devices based on multi-wire/channel Rashba semiconductors, which harbor Majorana fermions (MFs) *without* a Zeeman field. In contrast, magnetic fluxes, supercurrents or electric fields can be employed, yielding an enhanced device manipulability. The generic topological phase diagram for two-nanowire/channel systems, exhibits features of quantum criticality and a rich interplay of phases with 0, 1 or 2 MFs per edge. The most prominent and experimentally feasible implementation, relies on the already existing platforms of InAs-2DEG on top of a Josephson junction. Appropriate design of the latter device, allows phases with 1 or 2 MFs, both detectable in zero-bias anomaly peaks with a single or double unit of conductance. The absence of the Zeeman field in these devices could be assisting for a Kondo-peak-free interpretation.

PACS numbers: 74.78.-w, 74.45.+c, 85.25.-j

Introduction. The perspective of topological quantum computing (TQC) [1], has motivated a plethora of proposals for engineering topological superconductors (TSCs) based on semiconductors with strong Rashba spin-orbit coupling (SOC) [2–7]. Among them, a device involving a Rashba nanowire (NW) [3], lies in the spotlight of current research. The latter setup, requires a sufficiently strong Zeeman field in order to enter the TSC phase with 1MF per edge. The first encouraging zero bias anomaly (ZBA) MF-findings have been already reported [8, 9], which are however, still under debate [10].

A promising route for resolving this controversy is to explore alternative TSC platforms, which build upon the *same* materials used in these experiments, but with the Zeeman field replaced by some other control knob, such as a supercurrent flow or an electric field. The latter appear less harmful for the bulk SC and possibly more versatile for TQC. For instance, existing TQC protocols rely on sufficiently strong antiparallel magnetic fields, on a nanoscale level [11], which can be difficult to achieve in the lab. In contrast, harboring MFs *all-electrically*, can be advantageous for braiding and developing TSC-circuits. Notably, replacing the Zeeman field can also assist to exclude the possibility of a Kondo ZBA peak [10], leaving less room for misinterpreting MF fingerprints.

In this work, I propose a new type of artificial TSCs consisting of conventional SCs in proximity to *quasi-1d* semiconductors (with dimensions $L_x \gg L_y \gg L_z$), such as InAs and InSb. The quasi-1d nature of the semiconductor is instrumental for engineering a TSC *without* a Zeeman field [7]. As depicted in Fig. 1, the semiconductor can consist of either two NWs or a multi-channel film placed on top of a Josephson junction of two conventional SCs. A crucial requirement is to interrupt the interface separating the semiconductor from the SCs by an insulator, forming a loop (ABΓΔ). Via threading magnetic flux ($\Phi_{\rm flux}$) through this loop, MF bound states appear,

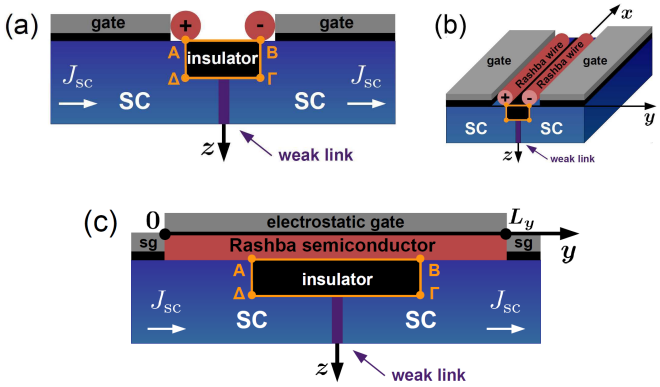

FIG. 1: (a)/(b) Side/Full view of two Rashba NWs and (c) Side view of a Rashba semiconducting film, both on top of a Josephson junction. The interface is interrupted by an insulating loop (ABΓΔ). Threading magnetic flux ($\Phi_{\rm flux}$) through the loop, leads to Majorana bound states extended along the y axis and localized at the edges along the x axis. The required magnetic flux can be generated by: **i.** a supercurrent flow ($J_{\rm sc}$) through the junction or **ii.** an electric field ($\mathcal{E}_{AB}$), generated by gates (sg) placed aside of the semiconductor.

which are localized at the edges of the primary dimension of the semiconductor (x axis) and extended along the secondary one (y axis). Aside from using a solenoid, one can generate the required flux via: **i.** a supercurrent flow $J_{\rm sc}$ through the Josephson junction or **ii.** an electric field $\mathcal{E}_{AB}$ generated by the side gates which contact the semiconductor, and act as a capacitor's plates. For the latter two implementations, the area of the loop can be infinitessimaly small. Remarkably, devices similar to the one in Fig. 1(c), have been already realized with InAs 2DEG [12], rendering the present proposal feasible.

Starting from a microscopic model, I first extract the generic topological diagram for this type of engineered TSCs. Both the two-NW and two-channel implementations which I consider here, can be mapped to each other and are characterized by a phase diagram supporting 0, 1 or 2 MFs per edge. The phase with 2MFs per edge is pro-

*Electronic address: panagiotis.kotetes@kit.edu

tected by chiral symmetry [5, 13] and meets the zero- and single- MF phases at two quantum tricritical points of the parameter space, which I identify. By adopting parameter values, representative of InAs and InSb, I make firm predictions for experimentally realizing and optimizing the present MF platforms. I find that the most promising device relies on a two-channel semiconducting film which supports both 1 and 2 MF-phases. On the other hand, two coupled NWs can harbor a single MF per edge *only* if they are in contact, while a single three-channel wire appears not to support MFs for the currently achieved promimity induced superconducting gap. For clarity, I discuss first the technically more transparent two-NW model, since the others can be mapped to it.

Two Rashba nanowires on top of a Josephson junction. For the implementation of Fig. 1(a), I consider the model Hamiltonian: $\mathcal{H} = \int \mathrm{d}x \left[\mathcal{H}_\psi(x) + \mathcal{H}_c(x) + \mathcal{H}_{\psi c}(x)\right]$ with:

$$\begin{aligned}
\mathcal{H}_\psi(x) &= \sum_{n=\pm} \hat{\psi}_n^\dagger \left[\varepsilon(\hat{p}_x) + v\hat{p}_x\sigma_y - neV_{AB}/2\right]\hat{\psi}_n \\
&+ \hat{\psi}_+^\dagger \left(t_\perp + iv_\perp\sigma_x\right) e^{i\frac{e}{\hbar}\Phi_{AB}}\hat{\psi}_- + \text{H.c.}\,, \qquad (1)\\
\mathcal{H}_c(x) &= \sum_{n=\pm} \hat{c}_n^\dagger \left[\tilde{\varepsilon}(\hat{p}_x) - neV_{\Delta\Gamma}/2\right]\hat{c}_n \\
&+ \tilde{t}_\perp e^{i\frac{e}{\hbar}\Phi_{\Delta\Gamma}}\hat{c}_+^\dagger\hat{c}_- + \sum_{n=\pm}\tilde{\Delta}e^{i\varphi_n}c_{n\uparrow}^\dagger c_{n\downarrow}^\dagger + \text{H.c.}\,, (2)\\
\mathcal{H}_{\psi c}(x) &= \mathrm{T}\left(e^{i\frac{e}{\hbar}\Phi_{A\Delta}}\hat{\psi}_+^\dagger\hat{c}_+ + e^{i\frac{e}{\hbar}\Phi_{B\Gamma}}\hat{\psi}_-^\dagger\hat{c}_-\right) + \text{H.c.}\,, \quad (3)
\end{aligned}$$

where in the above I suppressed the x argument of the fermionic field operators: $\hat{\psi}_n^\dagger(x) = (\psi_{n\uparrow}^\dagger(x)\,, \psi_{n\downarrow}^\dagger(x))$ and $\hat{c}_n^\dagger(x) = (c_{n\uparrow}^\dagger(x)\,, c_{n\downarrow}^\dagger(x))$, creating electrons on the NWs and the SCs, respectively. The $\boldsymbol{\sigma}$ Pauli matrices act on spin-space. The two parallel single-channel NWs, placed at distance L_y, are labelled with $n = \pm$ (see Fig. 1(a)). I also introduced: $\varepsilon(\hat{p}_x) = \hat{p}_x^2/2m - \mu$, $t_\perp$, v, $v_\perp$ denoting: kinetic energy measured from the chemical potential, inter-NW hopping, intra- and inter-NW SOC, correspondingly. Similarly, $\tilde{\varepsilon}(\hat{p}_x)$ and $\tilde{t}_\perp$ denote the respective terms for the electrons of the SCs. Furthermore, I included the spin-singlet superconducting order parameters $\tilde{\Delta}e^{i\varphi_\pm}$, where I assumed a phase difference $\delta\varphi = \varphi_+ - \varphi_-$, that *contributes* to a supercurrent flow ($J_{\rm sc}$) through the Josephson junction. I also added appropriate voltage drops (V_{ab}) and Peierls'-phases (Φ_{ab}), for all the pairwise coupled elements (a, b) of the hybrid device. Each cross-section of the hybrid device (see Fig. 2(a)), constitutes a superconducting quantum interference device, with the coupled NWs playing the role of the second weak link, similar to other experimentally realized setups [14].

Flux & Supercurrent. For the rest, I demand $V_{AB} = V_{\Delta\Gamma} = \Phi_{\Delta\Gamma} = \Phi_{A\Delta} = \Phi_{B\Gamma} = 0$, which according to Ref. [15], imposes: $\mathcal{E}_{AB} = \dot{\Phi}_{\rm flux}$, $\mathcal{E}_{\Delta\Gamma} = 0$, $\Phi_{AB} = -\Phi_{\rm flux}$, with the electric field $\mathcal{E}_{ab} = V_{ab} - \dot{\Phi}_{ab}$ (here $\dot{f} \equiv \partial f/\partial t$). We additionally obtain $\delta\varphi = J_{\rm sc}$, i.e., *equal* to the supercurrent $J_{\rm sc}$ flowing through the junction [16]. Thus only the gauge invariant quantities, $\Phi_{\rm flux}$ and $J_{\rm sc}$, appear in the Hamiltonian. Threading flux is usually achieved

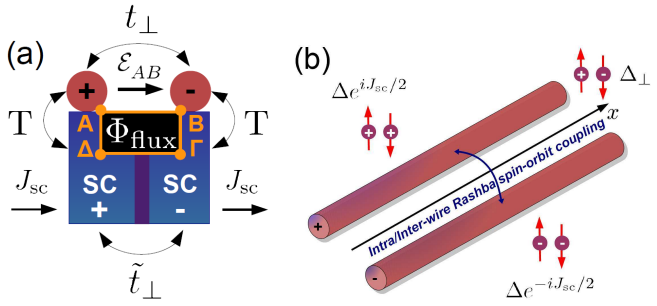

FIG. 2: (a) Cross-section of Fig. 1(b) with couplings: NW-NW ($t_\perp$), SC-SC ($\tilde{t}_\perp$), and NW-SC (T). Each cross-section behaves as a superconducting quantum interference device and the total system transits to a TSC phase for a sufficient amount of flux ($\Phi_{\rm flux}$). The required flux can be produced by an electric field $\mathcal{E}_{AB} \equiv \dot{\Phi}_{\rm flux}$ or a supercurrent $J_{\rm sc} \equiv 2e\Phi_{\rm flux}/\hbar$. (b) Induced multi-component superconducting gap on the NWs, when flux is generated by a supercurrent. For $J_{\rm sc} = \pi$, time-reversal symmetry *is violated*, since the intra- and inter-NW gaps exhibit a $\pi/2$-phase locking.

by employing a solenoid or an electric field yielding $\Phi_{\rm flux} = \int_{t_0}^{t} \mathrm{d}t' \mathcal{E}_{AB}(t')$. Nonetheless, in the particular setup it can alternatively arise via inducing a supercurrent flow equal to $J_{\rm sc} = 2e\Phi_{\rm flux}/\hbar$ [15]. Flux can be induced electrically using a capacitor (side gates) which discharges in the presence of an appropriately attached resistive circuit. A discharging initiated at t_0, leads to a flux $\Phi_{\rm flux} = \tau\mathcal{E}_{AB}(t_0)$, with τ the characteristic discharging time. Note that the supercurrent flow has to be kept zero during the discharging process. Conversely, we have to ensure that $\mathcal{E}_{AB} = 0$ when inducing flux via a supercurrent flow. Generally, the *simultaneous* control of both quantities is required for achieving a TSC.

Effective NW model. I proceed with integrating out the superconducting degrees of freedom, following Ref. [17]. For this, I will consider $\Phi_{AB} = -\Phi_{\rm flux} \equiv -\pi\phi$ and $\delta\varphi = J_{\rm sc} = 0$, where I introduced the normalized flux $\phi = \Phi_{\rm flux}/\Phi_0$ ($\Phi_0 = h/2e$). For the integration procedure, it is more convenient to introduce "bonding" and "anti-bonding" type of linear combinations for the electronic operators of the SCs: $\hat{c}_{b,a} = (\hat{c}_+ \pm \hat{c}_-)/\sqrt{2}$, with corresponding Fermi-level density of states, $\nu_{b,a}$. As a result, intra- and inter-NW spin-singlet superconducting pairing is proximity induced on the NWs, which reads: $\Delta\sum_n \psi_{n\uparrow}^\dagger\psi_{n\downarrow}^\dagger + \Delta_\perp(\psi_{+\uparrow}^\dagger\psi_{-\downarrow}^\dagger + \psi_{-\uparrow}^\dagger\psi_{+\downarrow}^\dagger) + \text{H.c.}$, with $\Delta_\perp = \Delta(\nu_b - \nu_a)/(\nu_b + \nu_a)$ (see [15]). The effective Hamiltonian for the NWs, leading to a TSC [7], reads:

$$\begin{aligned}
\widehat{\mathcal{H}}_{\rm TSC}(\hat{p}_x) &= \varepsilon(\hat{p}_x)\tau_z + v\hat{p}_x\tau_z\sigma_y - \Delta\tau_y\sigma_y \\
&+ \left(t_\perp\tau_z\kappa_x - v_\perp\kappa_y\sigma_x\right)e^{i\pi\phi\tau_z\kappa_z} - \Delta_\perp\tau_y\kappa_x\sigma_y\,, \quad (4)
\end{aligned}$$

where I employed the spinor $\widehat{\Psi}^\dagger(x) = (\psi_{+\uparrow}^\dagger(x),\ \psi_{+\downarrow}^\dagger(x),\ \psi_{-\uparrow}^\dagger(x),\ \psi_{-\downarrow}^\dagger(x),\ \psi_{+\uparrow}(x),\ \psi_{+\downarrow}(x),\ \psi_{-\uparrow}(x),\ \psi_{-\downarrow}(x))$. The $\boldsymbol{\tau}$ and $\boldsymbol{\kappa}$ Pauli matrices act on Nambu and NW ($\pm$) spaces. Note that if we had instead chosen $\Phi_{AB} = 0$ and

$\delta\varphi = J_{\rm sc} = 2\pi\phi$, we would have obtained an equivalent description sketched in Fig. 2(b), with the transformed intra-NW gaps $\Delta e^{\pm iJ_{\rm sc}/2}$, and the inter-NW gap $\Delta_\perp$.

Symmetry analysis. For investigating the symmetries of the Hamiltonian in Eq. (4), I will first consider $\phi = 1/2$ and $\Delta_\perp = 0$. In this case, the Hamiltonian enjoys the symmetries: $\Xi = \tau_x\mathcal{K}$ & $\widetilde{\Xi} = \tau_x\kappa_y\sigma_y\mathcal{K}$ (charge-conjugation), $\Theta = \kappa_x\mathcal{K}$ & $\widetilde{\Theta} = i\kappa_z\sigma_y\mathcal{K}$ (time-reversal) and $\Pi = \tau_x\kappa_x$ & $\widetilde{\Pi} = \tau_x\kappa_z\sigma_y$ (chiral). Here $\mathcal{K}$ denotes complex conjugation. Note that $\Xi^2 = \widetilde{\Xi}^2 = \Theta^2 = +I$ and $\widetilde{\Theta}^2 = -I$. Essentially $\widetilde{\Theta}$ effects the usual time-reversal symmetry ($\mathcal{T}$) leading to MF Kramers pairs. The two chiral symmetries lead to a unitary symmetry $\mathcal{O} \propto \Pi\widetilde{\Pi} = \kappa_y\sigma_y$, which commutes with the Hamiltonian, allowing its diagonalization into two sub-blocks. Via the unitary transformation $\mathcal{U} = (\kappa_z + \kappa_y\sigma_y)/\sqrt{2}$, I diagonalize $\mathcal{O}$ and obtain the two resulting $\kappa = \pm$ blocks, $\widehat{\mathcal{H}}^{\mathcal{U}}_\kappa(\hat{p}_x) = \varepsilon(\hat{p}_x)\tau_z + v\hat{p}_x\tau_z\sigma_y + \kappa t_\perp\sigma_y - v_\perp\tau_z\sigma_z - \Delta\tau_y\sigma_y$, describing two decoupled single-channel Rashba NWs in the presence of a superconducting gap Δ and an effective block dependent Zeeman field $\boldsymbol{\mathcal{B}}_\kappa = (0, \kappa t_\perp, -v_\perp)$, with parallel and perpendicular components to the SOC polarization. Both Hamiltonians belong to symmetry class D with the charge-conjugation symmetry Ξ. If the value of $t_\perp$ is such, so that the energy spectrum is fully gapped, each sub-subsystem harbors a single MF per edge when $\sqrt{t_\perp^2 + v_\perp^2} > \sqrt{\Delta^2 + \mu^2}$. Due to the underlying Kramers degeneracy, both subsystems become topological together, yielding a *$\mathcal{T}$-invariant TSC.*

The addition of $\Delta_\perp$ yields the BDI symmetry class with symmetries: $\{\Xi, \Theta, \Pi\}$. Consequently, a finite $\Delta_\perp$ ensures that we can obtain *at least* one MF per edge, *even* for $\delta\varphi = \pi$. In fact, for a finite supercurrent (as in Fig. 2(b)) realizing a π-junction, the intra-NW gaps become imaginary ($\pm i\Delta$) and the inter-NW gap remains real ($\Delta_\perp$). Thus the multi-component superconducting gap violates $\mathcal{T}$ intrinsically, offering a unique mechanism for obtaining single-MF phases *without* a Zeeman field.

TSC mechanism. The catalytic effect of the supercurrent (or flux) is reflected in the conversion of the inter-NW Rashba SOC, into the Zeeman term $v_\perp\tau_z\sigma_z$, which is complete for a π-junction [7]. The emergent Zeeman term is polarized perpendicular to the intra-NW SOC $v\hat{p}_x\tau_z\sigma_y$, akin to the situation encountered in strictly 1d NW-models [3]. In fact, the inter-NW SOC is here decisive for obtaining MFs, since the intra-NW SOC polarization is the same for both NWs. This is in stark contrast to the $\mathcal{T}$-preserving models of Ref. [6] where the inter-NW hopping becomes crucial. Note that a supercurrent flow has been also recently proposed in Ref. [18] as an indispensable ingredient for engineering a TSC, while other works [19, 20] have highlighted its role as a tool for either tailoring [19] or mapping [20] MF-phases.

Phase diagram. For investigating the related topological phase diagram, I rely on chiral symmetry and block off-diagonalize the Hamiltonian of Eq. (4) via the unitary transformation $(\tau_z + \tau_x\kappa_x)/\sqrt{2}$. I obtain the respective

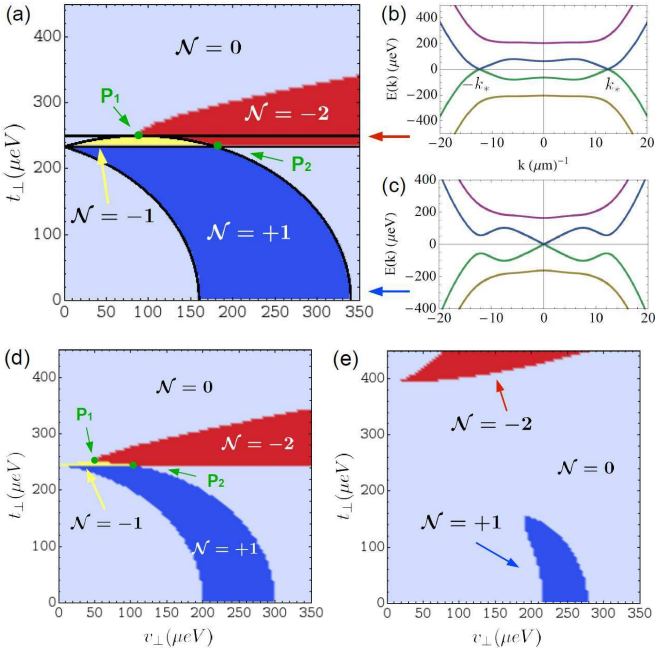

FIG. 3: Topological phase diagrams (TPDs), in $v_\perp - t_\perp$ plane, for InSb (InAs case is almost identical). Here $\mu = 0$ and $\Delta = 250\mu$eV. (a) TPD for $\Delta_\perp = 90\mu$eV and $\phi = 1/2$ ($J_{\rm sc} = \pi$). Four distinct phases appear with $\mathcal{N} = 0, \pm 1, 2$. $|\mathcal{N}|$ denotes the number of MFs per edge. The 1MF-phases (blue & yellow) are enclosed by the critical lines $\Delta^2 = t_\perp^2 + (\Delta_\perp \pm v_\perp)^2$, defined by the bulk gap closings at $k = 0$, with an example shown in (c) for $(v_\perp, t_\perp) = (300, 136)\mu$eV. The $\mathcal{N} = -2$ phase is protected by chiral symmetry and arises from gap closings at the inversion connected points, $\pm k_*$, with an example shown in (b) for $(v_\perp, t_\perp) = (300, 233)\mu$eV. The $\mathcal{N} = +1$ and $\mathcal{N} = -2$ phases, overlap, yielding a 1MF-phase with $\mathcal{N} = -1$. The latter region is enclosed by two parallel lines given by $t_\perp \simeq \sqrt{\Delta^2 - \Delta_\perp^2}$ and $t_\perp \simeq \Delta$. Thus two quantum tricritical points appear: $P_1 = (\Delta_\perp, \Delta)$ and $P_2 = (2\Delta_\perp, \sqrt{\Delta^2 - \Delta_\perp^2})$, where the phases with 0,1 and MFs per edge meet. (d) TPD for $\Delta_\perp = 50\mu$eV and $\phi = 1/2$. Results similar to (a), but with the window for the 1MF-phase suppressed, since it depends on $\Delta_\perp$. For $\Delta_\perp = 0$, the 1MF-phase disappears, since Kramers degeneracy is restored and only MF pairs are allowed. (e) TPD for $\Delta_\perp = 50\mu$eV and $\phi = 0.45$. Significantly away from the π-junction, the critical points $P_{1,2}$ vanish, as the $\mathcal{N} = +1$ and $\mathcal{N} = -2$ do not overlap anymore.

k-space Hamiltonian $\widehat{\mathcal{H}}'(k) = \tau_+\hat{A}(k) + \tau_-\hat{A}^\dagger(k)$, with the off-diagonal block projectors $\tau_\pm = (\tau_x \pm i\tau_y)/2$ and

$$\hat{A}(k) = \varepsilon(k)\kappa_x + v\hbar k\kappa_x\sigma_y + (v_\perp\sigma_x - it_\perp\kappa_z)\sin(\pi\phi) + (t_\perp + iv_\perp\kappa_z\sigma_x)\cos(\pi\phi) - i(\Delta + \Delta_\perp\kappa_x)\sigma_y\,. \quad (5)$$

The relevant $\mathbb{Z}$ topological invariant, $\mathcal{N}$, is defined as the winding number of $D(k) \equiv \mathrm{Det}[\hat{A}(k)]$ [5]. By employing the unit vector $\hat{\boldsymbol{g}}(k) = (0, D_\Im(k)/D(k), D_\Re(k)/D(k))$, $\mathcal{N}$ is defined as [18]

$$\mathcal{N} = \frac{1}{2\pi}\int dk\,\left(\hat{\boldsymbol{g}}(k) \times \frac{\partial\hat{\boldsymbol{g}}(k)}{\partial k}\right)_x . \quad (6)$$

In Fig. 3, I present a series of $v_\perp - t_\perp$ topological phase diagrams, obtained for $\mu = 0$ and representative values [8] for InSb NWs with proximity induced superconductivity, i.e. $v\hbar = 0.20$eVÅ, $m = 0.015m_e$ and $\Delta = 250\mu$eV. Fig. 3(a) was obtained for $\phi = 1/2$ and $\Delta_\perp = 90\mu$eV. Here we find three phases with 0, 1 or 2 MFs per edge. The phase with a single MF is bounded by the lines $\Delta^2 = t_\perp^2 + (\Delta_\perp \pm v_\perp)^2$, which are given by the gap closing condition for the inversion-symmetric wave-vector $k = 0$. A particular gap closing is shown in Fig. 3(c) for $(v_\perp, t_\perp) = (300, 136)\mu$eV. On the other hand, the phase with two MFs is associated with gap closings at two non-inversion-symmetric wave-vectors, $\pm k_*$, which are however connected by inversion. I present a relevant gap closing in Fig. 3(b) at $(v_\perp, t_\perp) = (300, 233)\mu$eV. The phase with 2 MFs is topologically protected, as long as chiral symmetry $\Pi = \tau_x\kappa_x$ persists [5]. This symmetry could be violated by a mismatch of the intra-NW gaps which would enter in Eq. (4) with a term $\sim \tau_y\kappa_z\sigma_y$.

For $(\hbar k)^2/2m \gg v\hbar k$, one finds that the gap closings at $\pm k_*$ occur at parts of the parallel lines $t_\perp \simeq \sqrt{\Delta^2 - \Delta_\perp^2}$ and $t_\perp \simeq \Delta$, shown in Fig. 3(a). It is straightforward to infer that the phases with $\mathcal{N} = +1$ (blue) and $\mathcal{N} = -2$ (red), overlap, leading to the phase with $\mathcal{N} = -1$ (yellow). As a result, two quantum tricritical points emerge (see also [21]), where the phases with 0, 1 and 2 MFs meet. The coordinates for these two points read: $P_1 \simeq (\Delta_\perp, \Delta)$ and $P_2 \simeq (2\Delta_\perp, \sqrt{\Delta^2 - \Delta_\perp^2})$. The phase diagram of Fig. 3(d(e)) was retrieved for $\Delta_\perp = 50\mu$eV and $\phi = 1/2(0.45)$. We observe that the tricritical points appear only for $\phi = 1/2$, while away from this value the TSC region becomes suppressed. Note also that if $t_\perp \simeq 0$, the window for a single MF-phase reads: $\Delta - \Delta_\perp < v_\perp < \Delta + \Delta_\perp$. Thus maximizing the inter-NW induced gap enhances the robustness of the TSC phase.

Predictions for experiments. In reality, the NWs have a finite diameter $d \sim 110$nm [8, 22]. If the NWs are in contact, we can assume $t_\perp \sim \hbar^2/(2mL_y^2)$ and $v_\perp \sim v\hbar/L_y$. In this case, for $\phi = 1/2$ and $\Delta_\perp = 90(50)\mu$eV, the 1MF-phase can be realized if $105\text{nm} < L_y < 150\text{nm}$ ($109\text{nm} < L_y < 131\text{nm}$). Setting instead $v\hbar = 0.15$eVÅ and $m = 0.024m_e$, allows us to address the InAs case. By rescaling k, one finds that the topological phase diagrams for InAs almost coincide with those of Fig. 3. For $\phi = 1/2$ and $\Delta_\perp = 90(50)\mu$eV, the 1MF-phase appears in InAs NWs for $82\text{nm} < L_y < 115\text{nm}$ ($86\text{nm} < L_y < 102\text{nm}$). Thus the 1MF-phase is accessible *only* when the NWs are placed *next to each other* ($L_y \simeq d$). Otherwise, $t_\perp$ and $v_\perp$ become much weaker, as they are given by the exponentially decaying overlap of the NW wavefunctions. Finally, the 2MF-phase appears experimentally inaccessible for the *particular* setup, since it would require for the NWs to be closer than their diameter ($L_y < d$).

Two-channel Rashba semiconducting film on top of a Josephson junction. Similar and even more promising results are obtained in the case of a two-channel Rashba semiconductor. For carrying out the analysis, I will here consider that the flux is generated electrically. Similar results can be obtained if a supercurrent flow is instead assumed. The effective Hamiltonian reads (see [15]):

$$\begin{aligned}\mathcal{H} &= \int d\boldsymbol{r}\, \hat{\psi}^\dagger(\boldsymbol{r}) \left[\frac{\hat{\boldsymbol{\pi}}^2}{2m} - \mu(t,y) + v\,(\hat{\boldsymbol{\pi}} \times \boldsymbol{\sigma}) \cdot \hat{\boldsymbol{z}}\right] \hat{\psi}(\boldsymbol{r}) \\ &+ \int d\boldsymbol{r} \left[\Delta(y)\psi_\uparrow^\dagger(\boldsymbol{r})\psi_\downarrow^\dagger(\boldsymbol{r}) + \text{H.c.}\right], \end{aligned} \tag{7}$$

with $\hat{\boldsymbol{\pi}} = \hat{\boldsymbol{p}} + e\boldsymbol{A} + \hbar\boldsymbol{\nabla}\varphi/2$. Here $\boldsymbol{A} = A_y\hat{\boldsymbol{y}}$ defines the vector potential in the film (equivalent to Φ_{AB}), while $\varphi = \varphi(t,y)$ is the phase of the bulk superconductor. Moreover, $\mu(t,y) = \mu - \hbar\dot{\varphi}/2 - U_{\text{conf}}(y) + eV_{\text{sg}}(t,y)$, consisting of a chemical potential μ, a phase contribution, a confining potential $U_{\text{conf}}(y)$ and the electrostatic side gate potential $V_{\text{sg}}(t,y)$. Here I consider an infinite well confining potential $U_{\text{conf}}(y) = +\infty$ for $y < 0$ and $y > L_y$, which yields the confinement channel wavefunctions $\langle y|n\rangle = \sqrt{2/L_y}\sin(n\pi y/L_y)$ with $n = 1, 2, \ldots$ and $\epsilon_n \equiv \langle n|\hat{p}_y^2/2m|n\rangle = (\hbar\pi n)^2/2mL_y^2$. The proximity induced superconducting gap $\Delta(y)$ is zero for $y \in [(L_y - b)/2, (L_y + b)/2]$ and equal to $\bar{\Delta}$ otherwise ($b \equiv$(AB); see Fig. 1(c)). The particular spatial profile is *required* for retrieving a $\mathcal{T}$-violating multi-component gap, similar to Δ and $\Delta_\perp$ encountered in the NW case.

For the present discussion, I will restrict to the lowest two confinement channels, $\{2, 1\}$, and employ the $\boldsymbol{\kappa}$ Pauli matrices for acting in their subspace. After effecting the unitary transformation $(\kappa_z + \kappa_x)/\sqrt{2}$, the corresponding Hamiltonian becomes identical to that of Eq. (4) with the following mappings [15]: $\mu \to \mu - 5\epsilon_1/2$, $t_\perp \to 3\epsilon_1/2$, $v_\perp \to -8v\hbar/3L_y$, $\Delta \to \Delta_c \equiv (\Delta_2 + \Delta_1)/2$, $\Delta_\perp \to \delta\Delta/2 \equiv (\Delta_2 - \Delta_1)/2$ and $\phi \to -(32L_y/9\pi^2\Phi_0)\int_{t_0}^t dt'\mathcal{E}_y(t')$, where I have introduced the superconducting gaps:

$$\Delta_c = \bar{\Delta}\left[1 - \frac{b}{L_y} - \frac{\sin(\pi b/L_y)}{\pi}\sin^2\left(\frac{\pi b}{2L_y}\right)\right], \tag{8}$$

$$\frac{\delta\Delta}{2} = \bar{\Delta}\frac{\sin(\pi b/L_y)}{\pi}\cos^2\left(\frac{\pi b}{2L_y}\right) \tag{9}$$

and $\Delta_n = \int_0^{L_y} dy\, \langle y|n\rangle^2\, \Delta(y)$, with $n = 1, 2$. At this point I will place the chemical potential symmetrically within ϵ_1 and ϵ_2, i.e. $\mu = 5\epsilon_1/2$, which is achieved by an appropriate gate voltage offset. This value has been proposed [4] as a sweet spot for two-channel models, at which the device becomes robust against charge fluctuations. Evenmore, we can maximize the TSC window via maximizing $\delta\Delta$. This occurs for $b/L_y = 1/3$, yielding $\Delta_c \simeq 3\bar{\Delta}/5$ and $\delta\Delta/2 \simeq \bar{\Delta}/5$, which I assume below.

Predictions for experiments. The most prominent realization of this setup is based on already existing 2DEG devices [12]. I assume that $\phi = 1/2$, while I set $\bar{\Delta} = 400\mu$eV, which implies $\Delta_c = 240\mu$eV and $\delta\Delta/2 = 80\mu$eV. Under these conditions, the 1MF-phase is stabilized for InAs when $315\text{nm} < L_y < 388\text{nm}$. On the other hand, for InSb the 1MF-phase appears for $400\text{nm} < L_y < 499\text{nm}$. In stark contrast to the double-NW case, here the 2MF-phase becomes experimentally

accessible, approximately when: 294nm $< L_y <$ 312nm for InAs and 370nm $< L_y <$ 395nm for InSb.

Three-channel Rashba nanowire on top of a Josephson junction. The above analysis can be extended to InSb nanowires, which appear to be multi-channel [8, 22]. Instead of a film, here I consider a single nanowire with square cross-section: $L_x \gg L_y = L_z = d \sim 110$nm [8]. The confinement channels are now labelled by (n, s), with $n(s)$ corresponding to the $y(z)$ axis sinusoidal wavefunctions [15]. The lowest energy level is the $(1, 1)$, while directly above that, we find the two degenerate levels $(2, 1)$ and $(1, 2)$. For Rashba SOC, only the levels $(2, 1)$ and $(1, 1)$ couple, and the level $(1, 2)$ can be neglected for the analysis of the topological properties [15]. As before, the 1MF-phase boundaries will be determined by the relations $\Delta^2 = t_\perp^2 + (\Delta_\perp \pm v_\perp)^2$.

Predictions for experiments. For $b = L_y/3$ and a chemical potential symmetrically placed inbetween the levels $(2, 1)$ and $(1, 1)$, I find that the 1MF-phase is realized for a proximity induced gap: 5.2meV $< \bar{\Delta} <$ 5.8meV. Thus it seems currently impossible to engineer a TSC with a single InSb wire, via the proposed mechanism. The reason is the large energy splitting $\sim$ 3meV of the two coupled channels, compared to the recently experimentally achieved induced superconducting gap $\sim$ 0.6meV [22].

Conclusions. To summarize, I proposed a new class of MF platforms, relying on *quasi-1d* semiconductors. The particular dimensionality allows *replacing* the Zeeman field with supercurrents or electric fields. Double-nanowire setups, which can support 1MF-phases when the nanowires are parallel and in contact to each other, appear experimentally accessible [22]. In contrast, a single multi-channel InSb nanowire can not be used for harboring MFs with the currently achieved proximity induced superconducting gaps. However, there are other multi-channel implementations promising experimental feasibility and enhanced versatility. In fact, InAs 2DEG devices in proximity to a Josephson junction have been already achieved three decades ago, and constitute ideal candidates for realizing the particular MF proposal. According to the present analysis, they can exhibit an interplay of phases with 1 or 2 MFs per edge, depending on the width of the device. The MF-window is optimized when the proximity effect is interrupted for a width (AB)$= L_y/3$. Further optimization requires a supercurrent value of $J_{\rm sc} = \pi$, which could be imposed by connecting the Josephson junction to a large superconducting ring pierced by a suitable amount of flux. Alternatively, an electric field $\tau \mathcal{E}_y(t_0) L_y = 9\pi^2 \Phi_0/64$ can be applied across the film. For $\tau \sim 1\mu s$(ns) and $L_y \sim 400$nm, a weak field $\sim 70\mu$V(mV)/cm is required, opening new perspectives for *all-electrical* control on MF devices.

I am glad to thank A. Shnirman, G. Schön, A. Geresdi, R. Aguado, V. Mourik, E. Prada, A. Heimes, D. Pikulin, M. Wimmer, J. Schmalian, P.-Q. Jin and D. Mendler for valuable discussions and suggestions which significantly helped me to improve and complete this work.

[1] A. Yu. Kitaev, Annals Phys. **303**, 2 (2003); C. Nayak *et al.*, Rev. Mod. Phys. **80**, 1083 (2008); N. Read and D. Green, Phys. Rev. B **61**, 10267 (2000); A. Yu. Kitaev, Phys.-Usp. **44**, 131 (2001); D. A. Ivanov, Phys. Rev. Lett. **86**, 268 (2001); L. Fu and C. L. Kane, *ibid.* **100**, 096407 (2008); J. Alicea *et al.*, Nat. Phys. **7** 412 (2011); J. Alicea, Rep. Prog. Phys. **75**, 076501 (2012); C. W. J. Beenakker, Annu. Rev. Con. Mat. Phys. **4**, 113 (2013).

[2] J. D. Sau *et al.*, Phys. Rev. Lett. **104**, 040502 (2010); J. Alicea, Phys. Rev. B **81** 125318 (2010).

[3] R. M. Lutchyn, J. D. Sau and S. Das Sarma, Phys. Rev. Lett. **105**, 077001 (2010); Y. Oreg, G. Refael and F. von Oppen, Phys. Rev. Lett. **105**, 177002 (2010).

[4] R. M. Lutchyn, T. Stanescu, S. Das Sarma, Phys. Rev. Lett. **106**, 127001 (2011).

[5] S. Tewari and J. D. Sau, Phys. Rev. Lett. **109**, 150408 (2012).

[6] A. Keselman *et al.*, Phys. Rev. Lett. **111**, 116402 (2013); E. Gaidamauskas, J. Paaske, and K. Flensberg, Phys. Rev. Lett. **122**, 126402 (2014).

[7] P. Kotetes, New J. Phys. **15**, 105027 (2013).

[8] V. Mourik *et al.*, Science **336**, 1003 (2012).

[9] M. T. Deng *et al.*, Nano Lett. **12**, 6414 (2012); L. P. Rokhinson, Xinyu Liu, and J. K. Furdyna, *ibid.* **8**, 795 (2012); A. Das *et al.*, *ibid.* **8**, 887 (2012).

[10] E. J. H. Lee *et al.*, Phys. Rev. Lett. **109**, 186802 (2012); A. D. K. Finck *et al.*, *ibid.* **110**, 126406 (2013); H. O. H. Churchill *et al.*, Phys. Rev. B **87**, 241401(R) (2013); E. J. H. Lee *et al.*, Nat. Nanotechnol. **9**, 79 (2014).

[11] M. Leijnse and K. Flensberg, Phys. Rev. Lett. **107**, 210502 (2011).

[12] H. Takayanagi and T. Kawakami, Phys. Rev. Lett. **54**, 2449 (1985); M. Thomas *et al.*, Phys. Rev. B **58**, 11676 (1998).

[13] H.-Y. Hui *et al.*, 1407.7519.

[14] J.-P. Cleuziou *et al.*, Nature Nanotechnol. **1**, 53 (2006).

[15] Supplemental material attached.

[16] G. Schön and A. D. Zaikin, *Quantum Coherent Effects, Phase Transitions and Dissipative Dynamics of Ultra Small Tunnel Junctions*, PHYSICS REPORTS (Review Section of Physics Letters) **198**, Nos. 5 & 6, 237-412 North-Holland (1990).

[17] T. D. Stanescu *et al.*, Phys. Rev. B **81**, 241310(R) (2010); A. C. Potter and P. A. Lee, *ibid.* **83**, 184520 (2011).

[18] A. Heimes, P. Kotetes, and G. Schön, Phys. Rev. B **90**, 060507(R) (2014).

[19] B. Seradjeh and E. Grosfeld Phys. Rev. B **83**, 174521 (2011); A. Romito *et al.*, Phys. Rev. B **85**, 020502 (2012); X.-J. Liu and A. M. Lobos, *ibid.* **87**, 060504 (2013); J. Röntynen and T. Ojanen, arXiv:1406.4288.

[20] P. San-Jose, E. Prada and R. Aguado, Phys. Rev. Lett. **112**, 137001 (2014).

[21] R. M. Lutchyn and M. P. A. Fisher, Phys. Rev. B **84**, 214528 (2011).

[22] S. R. Plissard *et al.*, Nature Nanotechnol. **8**, 859 (2013).

Supplemental Material

Appendix A: Gauge transformation properties of the double nanowire Hamiltonian: Flux & Supercurrent

For clarity, I write here in an extended form the Hamiltonian presented in the manuscript, concerning the setup involving the two single-channel nanowires:

$$\mathcal{H}_{\psi}(x) = \sum_{n=\pm}\hat{\psi}_n^{\dagger}\left[\varepsilon(\hat{p}_x)+v\hat{p}_x\sigma_y-ne\frac{V_{AB}}{2}\right]\hat{\psi}_n+\hat{\psi}_+^{\dagger}\left(t_{\perp}+iv_{\perp}\sigma_x\right)e^{i\frac{e}{\hbar}\Phi_{AB}}\hat{\psi}_-+\hat{\psi}_-^{\dagger}\left(t_{\perp}-iv_{\perp}\sigma_x\right)e^{-i\frac{e}{\hbar}\Phi_{AB}}\hat{\psi}_+\,, \quad \text{(A1)}$$

$$\mathcal{H}_{c}(x) = \sum_{n=\pm}\left\{\hat{c}_n^{\dagger}\left[\tilde{\varepsilon}(\hat{p}_x)-ne\frac{V_{\Delta\Gamma}}{2}\right]\hat{c}_n+\tilde{\Delta}\left(e^{i\varphi_n}c_{n\uparrow}^{\dagger}c_{n\downarrow}^{\dagger}+e^{-i\varphi_n}c_{n\downarrow}c_{n\uparrow}\right)\right\}+\tilde{t}_{\perp}\left(e^{i\frac{e}{\hbar}\Phi_{\Delta\Gamma}}\hat{c}_+^{\dagger}\hat{c}_-+e^{-i\frac{e}{\hbar}\Phi_{\Delta\Gamma}}\hat{c}_-^{\dagger}\hat{c}_+\right), \quad \text{(A2)}$$

$$\mathcal{H}_{\psi c}(x) = \mathrm{T}\left(e^{i\frac{e}{\hbar}\Phi_{A\Delta}}\hat{\psi}_+^{\dagger}\hat{c}_++e^{i\frac{e}{\hbar}\Phi_{B\Gamma}}\hat{\psi}_-^{\dagger}\hat{c}_-+e^{-i\frac{e}{\hbar}\Phi_{A\Delta}}\hat{c}_+^{\dagger}\hat{\psi}_++e^{-i\frac{e}{\hbar}\Phi_{B\Gamma}}\hat{c}_-^{\dagger}\hat{\psi}_-\right). \quad \text{(A3)}$$

To ensure full generality I have added appropriate voltage drops (V_{ab}) and Peierls'-phases (Φ_{ab}), for all the pairwise coupled elements (a,b) of the hybrid device. Note that for compactness I have suppressed the x dependence of the field operators.

In order to illustrate the connection between the flux piercing the loop ABΓΔ and the supercurrent flow, I perform the following gauge transformation $\hat{\psi}_n(x)=e^{nie\chi/2\hbar}\hat{\psi}'_n(x)$ and $\hat{c}_n(x)=e^{nie\alpha/2\hbar}\hat{c}'_n(x)$, with χ and α independent of x. In the new gauge: $V'_{AB}=V_{AB}-\dot{\chi}$, $\Phi'_{AB}=\Phi_{AB}-\chi$, $V'_{\Delta\Gamma}=V_{\Delta\Gamma}-\dot{\alpha}$, $\Phi'_{\Delta\Gamma}=\Phi_{\Delta\Gamma}-\alpha$, $\Phi'_{A\Delta}=\Phi_{A\Delta}-(\chi-\alpha)/2$, $\Phi'_{B\Gamma}=\Phi_{B\Gamma}+(\chi-\alpha)/2$ and $\varphi'_n=\varphi_n-ne\alpha/\hbar$, where $\dot{f}$ denotes the time derivative of f. To this end, I demand: $V'_{AB}=V'_{\Delta\Gamma}=\Phi'_{\Delta\Gamma}=\Phi'_{A\Delta}=\Phi'_{B\Gamma}=0$, which imposes: $\mathcal{E}_{AB}=\dot{\Phi}_{\text{flux}}$, $\mathcal{E}_{\Delta\Gamma}=0$, $\Phi'_{AB}=\Phi_{AB}-\chi\equiv-\Phi_{\text{flux}}$, $\varphi'_n=\varphi_n-ne\alpha/\hbar\equiv\varphi_n-ne\Phi_{\Delta\Gamma}/\hbar$, with the electric field $\mathcal{E}_{ab}=V_{ab}-\dot{\Phi}_{ab}$. We additionally obtain $\delta\varphi'=\delta\varphi-2e\Phi_{\Delta\Gamma}/\hbar=J_{\text{sc}}$, i.e., equal to the supercurrent J_{sc} flowing through the junction [1]. Thus only $\Phi'_{AB}\equiv-\Phi_{\text{flux}}$ and $\delta\varphi'\equiv J_{\text{sc}}$, persist in the gauged Hamiltonian, which is the one that has been considered in the manuscript.

For the rest, I will consider that Φ_{flux} and J_{sc} are time-independent. In the steady state, their connection can be demonstrated by performing the additional gauge transformation $\chi\to\chi-\Phi_{\text{flux}}$ and $\alpha\to\alpha-\Phi_{\text{flux}}$, yielding $\Phi_{\text{flux}}\to0$ and $J_{\text{sc}}\to J_{\text{sc}}+2e\Phi_{\text{flux}}/\hbar$. Therefore, threading flux Φ_{flux}, which is usually achieved by employing a solenoid or an electric field yielding $\Phi_{\text{flux}}=\int_{t_0}^{t}\mathrm{d}t'\mathcal{E}_{AB}(t')$, is also equivalent to effecting a supercurrent flow equal to $J_{\text{sc}}=2e\Phi_{\text{flux}}/\hbar$.

Appendix B: Proximity induced superconductivity on the nanowires

The total Hamiltonian of the system reads $\mathcal{H}=\int\mathrm{d}x\left[\mathcal{H}_{\psi}(x)+\mathcal{H}_{c}(x)+\mathcal{H}_{\psi c}(x)\right]$. For retrieving the proximity induced superconducting gap, one has to integrate out the superconducting degrees of freedom. Here I will follow the method of Refs. [2]. For the integration, I consider that $J_{sc}=0$ and only a flux Φ_{flux} is finite. At this point, I focus on the last two parts of the complete Hamiltonian

$$\mathcal{H}_{c}(x) = \sum_{n=\pm}\left[\hat{c}_n^{\dagger}\left(\frac{\hat{p}_x^2}{2\tilde{m}}-\tilde{\mu}\right)\hat{c}_n+\tilde{\Delta}\left(c_{n\uparrow}^{\dagger}c_{n\downarrow}^{\dagger}+c_{n\downarrow}c_{n\uparrow}\right)\right]+\tilde{t}_{\perp}\left(\hat{c}_+^{\dagger}\hat{c}_-+\hat{c}_-^{\dagger}\hat{c}_+\right), \quad \text{(B1)}$$

$$\mathcal{H}_{\psi c}(x) = \mathrm{T}\left(\hat{\psi}_+^{\dagger}\hat{c}_++\hat{\psi}_-^{\dagger}\hat{c}_-+\hat{c}_+^{\dagger}\hat{\psi}_++\hat{c}_-^{\dagger}\hat{\psi}_-\right) \quad \text{(B2)}$$

and transfer to the bonding and anti-bonding basis $\hat{c}_{b,a}=(\hat{c}_+\pm\hat{c}_-)/\sqrt{2}$, which yields

$$\mathcal{H}_{c}(x) = \sum_{n=a,b}\left[\hat{c}_n^{\dagger}\left(\frac{\hat{p}_x^2}{2\tilde{m}}-\tilde{\mu}_n\right)\hat{c}_n+\tilde{\Delta}\left(c_{n\uparrow}^{\dagger}c_{n\downarrow}^{\dagger}+c_{n\downarrow}c_{n\uparrow}\right)\right], \quad \text{(B3)}$$

$$\mathcal{H}_{\psi c}(x) = \mathrm{T}\left[\left(\frac{\hat{\psi}_++\hat{\psi}_-}{\sqrt{2}}\right)^{\dagger}\hat{c}_b+\left(\frac{\hat{\psi}_+-\hat{\psi}_-}{\sqrt{2}}\right)^{\dagger}\hat{c}_a+\text{H.c.}\right], \quad \text{(B4)}$$

with $\tilde{\mu}_b=\tilde{\mu}-\tilde{t}_{\perp}$ and $\tilde{\mu}_a=\tilde{\mu}+\tilde{t}_{\perp}$. The latter difference in chemical potentials, leads to different density of states at the Fermi level, $\nu_{b,a}$. Moreover, in this new diagonalized basis, the bonding and anti-bonding fermions of the superconductor can be integrated out independently, exactly as prescribed in [2]. In the latter works, it has been additionally shown that the corresponding proximity induced gaps, Δ_b and Δ_a, are proportional to the density of

states $\nu_{b,a}$. By neglecting for the present discussion the arising renormalization effects [2], we obtain the proximity induced superconducting gaps on the nanowires

$$\Delta_b \frac{\psi^\dagger_{+\uparrow}+\psi^\dagger_{-\uparrow}}{\sqrt{2}}\frac{\psi^\dagger_{+\downarrow}+\psi^\dagger_{-\downarrow}}{\sqrt{2}}+\Delta_a \frac{\psi^\dagger_{+\uparrow}-\psi^\dagger_{-\uparrow}}{\sqrt{2}}\frac{\psi^\dagger_{+\downarrow}-\psi^\dagger_{-\downarrow}}{\sqrt{2}}+\text{H.c.}=\Delta\sum_{n=\pm}\psi^\dagger_{n\uparrow}\psi^\dagger_{n\downarrow}+\Delta_\perp(\psi^\dagger_{+\uparrow}\psi^\dagger_{-\downarrow}+\psi^\dagger_{-\uparrow}\psi^\dagger_{+\downarrow})+\text{H.c.}\,, \tag{B5}$$

with $\Delta=(\Delta_b+\Delta_a)/2$ and $\Delta_\perp=(\Delta_b-\Delta_a)/2$. By taking into account that $\Delta_{b,a}\propto\nu_{b,a}$, we obtain the relation presented in the manuscript: $\Delta_\perp=\Delta(\nu_b-\nu_a)/(\nu_b+\nu_a)$.

Appendix C: Effective Hamiltonian for the setup involving a two-channel Rashba semiconducting film

The effective Hamiltonian for this hybrid device, also presented in the manuscript, has the form:

$$\begin{aligned}\mathcal{H} &= \int d\boldsymbol{r}\;\hat{\psi}^\dagger(\boldsymbol{r})\left\{\frac{\left(\hat{\boldsymbol{p}}+e\boldsymbol{A}+\hbar\boldsymbol{\nabla}\varphi/2\right)^2}{2m}-\mu+U_{\text{conf}}(y)-eV_{\text{sg}}(t,y)+\frac{\hbar\dot{\varphi}}{2}+v\left[\left(\hat{\boldsymbol{p}}+e\boldsymbol{A}+\hbar\boldsymbol{\nabla}\varphi/2\right)\times\boldsymbol{\sigma}\right]\cdot\hat{\boldsymbol{z}}\right\}\hat{\psi}(\boldsymbol{r})\\ &+\int d\boldsymbol{r}\;\Delta(y)\left[\psi^\dagger_\uparrow(\boldsymbol{r})\psi^\dagger_\downarrow(\boldsymbol{r})+\psi_\downarrow(\boldsymbol{r})\psi_\uparrow(\boldsymbol{r})\right]\,.\end{aligned} \tag{C1}$$

The present effective Hamiltonian has been retrieved by integrating out the superconducting degrees of freedom as in Sec. B and according to Ref. [2]. Furthermore, a particular gauge has been chosen, so that the supercurrent J_{sc} and the electric field across the Josephson junction are *zero*, similarly to the discussion of Sec. A. Here $\boldsymbol{A}=A_y\hat{\boldsymbol{y}}$ defines the vector potential inside the semiconducting film (equivalent to Φ_{AB}), while $\varphi=\varphi(t,y)$ constitutes the phase of the bulk superconductor. The spatial dependence of the superconducting phase yields $\boldsymbol{\nabla}\varphi=\partial_y\varphi\hat{\boldsymbol{y}}$. By additionally assuming conditions equivalent to $\Phi_{A\Delta}=\Phi_{B\Gamma}=0$, i.e. the vector potential across the interface is zero, we obtain

$$\int_0^{L_y}\left(A_y+\frac{\hbar}{2e}\frac{\partial\varphi}{\partial y}\right)dy=-\Phi_{\text{flux}}\,. \tag{C2}$$

Similarly to the nanowire case, if we set $V_{\text{sg}}(t,y)=\hbar\dot{\varphi}/2e$, we obtain $\int_0^{L_y}\mathcal{E}_y dy=\dot{\Phi}_{\text{flux}}$.

The consideration of an infinite well confining potential $U_{\text{conf}}(y)=+\infty$ for $y<0$ and $y>L_y$, allows us to introduce the confinement channel wavefunctions $\langle y|n\rangle=\sqrt{2/L_y}\sin(n\pi y/L_y)$ with $n=1,2,\ldots$ and $\epsilon_n\equiv\langle n|\hat{p}_y^2/2m|n\rangle=(\hbar\pi n)^2/2mL_y^2$. The latter can be employed as a basis for expanding the field operators. By focusing on the two lowest confinement channels, we obtain an approximate Hamiltonian. Care has to be taken, so that the approximate Hamiltonian follows the same gauge transformation rules as the parent Hamiltonian of Eq. C1. In fact, the minimal coupling scheme $\hat{\boldsymbol{p}}\to\hat{\boldsymbol{p}}+e\boldsymbol{A}$ must be properly modified. For this reason, I first project the Hamiltonian of Eq. C1 onto the lowest confinement channels, for $V_{\text{sg}}=A_y=\varphi=0$. This yields

$$\widehat{\mathcal{H}}_{\text{film}}(\hat{p}_x)=\left(\frac{\hat{p}_x^2}{2m}-\mu+\frac{\epsilon_2+\epsilon_1}{2}\right)\tau_z+v\hat{p}_x\tau_z\sigma_y+\frac{\epsilon_2-\epsilon_1}{2}\,\tau_z\kappa_z-\frac{8v\hbar}{3L_y}\kappa_y\sigma_x-\frac{\Delta_2+\Delta_1}{2}\,\tau_y\sigma_y-\frac{\Delta_2-\Delta_1}{2}\,\tau_y\kappa_z\sigma_y\,, \tag{C3}$$

with the $\boldsymbol{\kappa}$ Pauli matrices acting on the subspace $\{2,1\}$ and $\Delta_n=\int_0^{L_y}dy\,\langle y|n\rangle^2\,\Delta(y)$ given by

$$\Delta_2=\bar{\Delta}\left[1-\frac{b}{L_y}+\frac{\sin(\pi b/L_y)}{\pi}\cos(\pi b/L_y)\right]\qquad\text{and}\qquad\Delta_1=\bar{\Delta}\left[1-\frac{b}{L_y}-\frac{\sin(\pi b/L_y)}{\pi}\right]\,. \tag{C4}$$

In order to introduce the gauge potentials, I will first retrieve the expression for the polarization operator in this basis. The polarization operator reads $P_y=-ey$ and in this basis has the representation $P_y=16eL_y\tau_z\kappa_x/9\pi^2$. In the presence of a homogeneous time-dependent electric field, $\mathcal{E}_y$, the Hamiltonian acquires an additional $-P_y\mathcal{E}_y$ term. In the latter case, we can infer the coupling of the two-channel system with the electrostatic potential and the superconducting phase, which reads, $P_y\partial_y(V_{\text{sg}}-\hbar\dot{\varphi}/2e)$. Here we assume that the gradients of the electrostatic potential and superconducting phase are constants. To retrieve the coupling to the vector potential, A_y, we have to first obtain the expression for the paramagnetic current operator $J_y=\dot{P}_y$. The latter time derivative can be retrieved using the Heisenberg equation of motion for the polarization operator, calculated using the non-superconducting, and therefore gauge invariant, part of the Hamiltonian in Eq. C3. Thus, we have

$$\begin{aligned}J_y &= \frac{i}{\hbar}\left[\left(\frac{\hat{p}_x^2}{2m}-\mu+\frac{\epsilon_2+\epsilon_1}{2}\right)\tau_z+v\hat{p}_x\tau_z\sigma_y+\frac{\epsilon_2-\epsilon_1}{2}\,\tau_z\kappa_z-\frac{8v\hbar}{3L_y}\kappa_y\sigma_x,\frac{16eL_y}{9\pi^2}\tau_z\kappa_x\right]\\ &= -\frac{2}{\hbar}\frac{16eL_y}{9\pi^2}\left(\frac{\epsilon_2-\epsilon_1}{2}\,\kappa_y+\frac{8v\hbar}{3L_y}\tau_z\kappa_z\sigma_x\right)\,.\end{aligned} \tag{C5}$$

The current above provides the linear correction to the Hamiltonian with respect to $A_y + \hbar\partial_y\varphi/2e$. Consequently, the interchannel terms become modified in the following manner

$$\begin{aligned}\frac{\epsilon_2-\epsilon_1}{2}\,\tau_z\kappa_z - \frac{8v\hbar}{3L_y}\kappa_y\sigma_x \;\rightarrow\; & \frac{\epsilon_2-\epsilon_1}{2}\,\tau_z\kappa_z - \frac{8v\hbar}{3L_y}\kappa_y\sigma_x - J_y\big(A_y+\hbar\partial_y\varphi/2e\big) \\ = \; & \left(\frac{\epsilon_2-\epsilon_1}{2}\,\tau_z\kappa_z - \frac{8v\hbar}{3L_y}\kappa_y\sigma_x\right)\left[1+i\frac{2}{\hbar}\frac{16eL_y}{9\pi^2}\left(A_y+\frac{\hbar}{2e}\frac{\partial\varphi}{\partial y}\right)\tau_z\kappa_x\right]. \end{aligned} \tag{C6}$$

The above linear term is useful for calculating the linear response to the external fields, e.g. conductivities, but can not yield the desired gauge transformation properties. To serve the latter purpose, it has to get exponentiated, i.e.

$$\frac{\epsilon_2-\epsilon_1}{2}\,\tau_z\kappa_z - \frac{8v\hbar}{3L_y}\kappa_y\sigma_x \quad\rightarrow\quad \left(\frac{\epsilon_2-\epsilon_1}{2}\,\tau_z\kappa_z - \frac{8v\hbar}{3L_y}\kappa_y\sigma_x\right)\mathrm{Exp}\left(-i\frac{32}{9\pi^2}\frac{e\Phi_{\rm flux}}{\hbar}\tau_z\kappa_x\right), \tag{C7}$$

where I additionally made use of Eq. C2 by considering that A_y is spatially homogeneous. If we now set the total electrostatic potential to zero, i.e. $V_{\rm sg}-\hbar\dot{\varphi}/2e=0$, Eq. C2 additionally provides $L_y\mathcal{E}_y = \dot{\Phi}_{\rm flux} \Rightarrow \Phi_{\rm flux} = L_y\int_{t_0}^{t} dt'\mathcal{E}_y(t')$. Therefore, the normalized flux in the particular case reads $\phi = -(32/9\pi^2)\Phi_{\rm flux}/\Phi_0$, with $\Phi_0 = h/2e$. We immediately notice the difference compared to the nanowire case, in which $\phi = \Phi_{\rm flux}/\Phi_0$. The projection to the lowest two confinement channels yields an effective flux piercing the loop $AB\Gamma\Delta$, equal to $-32\Phi_{\rm flux}/9\pi^2 \simeq -0.36\Phi_{\rm flux}$.

Under the aforementioned conditions and after effecting the unitary transformation $(\kappa_z+\kappa_x)/\sqrt{2}$, the Hamiltonian becomes

$$\widehat{\mathcal{H}}_{\rm film}(\hat{p}_x) = \left[\frac{\hat{p}_x^2}{2m} - \left(\mu - \frac{5\epsilon_1}{2}\right)\right]\tau_z + v\hat{p}_x\tau_z\sigma_y + \left(\frac{3\epsilon_1}{2}\tau_z\kappa_x + \frac{8v\hbar}{3L_y}\kappa_y\sigma_x\right)e^{i\pi\phi\tau_z\kappa_z} - \Delta_c\tau_y\sigma_y - \frac{\delta\Delta}{2}\,\tau_y\kappa_x\sigma_y\,, \tag{C8}$$

with $\Delta_c = (\Delta_2+\Delta_1)/2$ and $\delta\Delta = \Delta_2-\Delta_1$. Therefore, this Hamiltonian can be mapped to the one of Eq. (4) of the manuscript, where the parameters of Eq. (4) correspond to: $\mu \to \mu - 5\epsilon_1/2$, $t_\perp \to 3\epsilon_1/2$, $v_\perp \to -8v\hbar/3L_y$, $\phi \to -(32L_y/9\pi^2\Phi_0)\int_{t_0}^{t} dt'\mathcal{E}_y(t')$, $\Delta \to \Delta_c$ and $\Delta_\perp \to \delta\Delta/2$.

Appendix D: Effective Hamiltonian for the setup involving a three-channel Rashba semiconducting wire

In this paragraph I derive the effective Hamiltonian for a hybrid device involving a three-dimensional Rashba semiconducting wire, where three confinement channels have to be taken into account within a low energy description. For simplicity, I will here consider a wire with square cross-section $L_y = L_z \equiv d$. As I show below, out of the three channels, only two are coupled and can lead to non-trivial topological properties, as in the purely two-channel case of a semiconducting film. The remaining channel decouples and cannot support Majorana fermions. The derivation will be performed first for $A_y = \varphi = V_{\rm sg} = 0$. The starting point is the Hamiltonian

$$\mathcal{H} = \int d\boldsymbol{r}\;\hat{\psi}^\dagger(\boldsymbol{r})\left[\frac{\hat{\boldsymbol{p}}^2}{2m} - \mu + U_{\rm conf}(y,z) + v\,(\hat{\boldsymbol{p}}\times\boldsymbol{\sigma})\cdot\hat{\boldsymbol{z}}\right]\hat{\psi}(\boldsymbol{r}) + \int d\boldsymbol{r}\;\Delta(y)\left[\psi_\uparrow^\dagger(\boldsymbol{r})\psi_\downarrow^\dagger(\boldsymbol{r}) + \psi_\downarrow(\boldsymbol{r})\psi_\uparrow(\boldsymbol{r})\right]. \tag{D1}$$

Here I assumed that the superconducting gap varies only with y, due to the blocked proximity effect by an insulating layer as in the case of the semiconducting film. The consideration of an infinite well confining potential $U_{\rm conf}(z,y)=0$ for $\{y,z\}\in\{[0,d],[0,d]\}$ and $+\infty$ otherwise, allows us to introduce the confinement channel wavefunctions $\langle y,z|n,s\rangle = (2/d)\sin(n\pi y/d)\sin(s\pi y/d)$ with $n,s=1,2,\ldots$ and $\epsilon_{n,s} \equiv \langle n,s|\left(\hat{p}_y^2+\hat{p}_z^2\right)/2m|n,s\rangle = (\hbar\pi)^2(n^2+s^2)/2md^2$. The latter can be employed as a basis for expanding the field operators. In order to focus on the low energy sector of the Hamiltonian, the three lowest channels have to be taken into account. The energetically lowest level is $(1,1)$ while the two above, $(2,1)$ and $(1,2)$, are degenerate. This yields

$$\begin{aligned}\widehat{\mathcal{H}}_{\rm wire}(\hat{p}_x) \;=\; & \left(\frac{\hat{p}_x^2}{2m} - \mu + \epsilon_1 + \frac{\epsilon_2+\epsilon_1}{2}\right)\tau_z + v\hat{p}_x\tau_z\sigma_y + \frac{\epsilon_2-\epsilon_1}{2}\,\tau_z\begin{pmatrix}1&0&0\\0&1&0\\0&0&-1\end{pmatrix} - \frac{8v\hbar}{3L_y}\begin{pmatrix}0&0&0\\0&0&-i\\0&i&0\end{pmatrix}\sigma_x \\ - \; & \frac{\Delta_2+\Delta_1}{2}\,\tau_y\sigma_y - \frac{\Delta_2-\Delta_1}{2}\,\tau_y\begin{pmatrix}-1&0&0\\0&1&0\\0&0&-1\end{pmatrix}\sigma_y\,, \end{aligned} \tag{D2}$$

with the basis $\{(1,2),(2,1),(1,1)\}$. Note that I used $\epsilon_{1,2}$ and $\Delta_{1,2}$ defined in Sec. C, with $L_y = d$. As seen above, in the absence of gauge potentials, the channel $(1,2)$ decouples from the other two. In order to infer if this situation

persists for finite gauge potentials, I calculate the polarization operators $P_y = -ey$ and $P_z = -ez$ in this basis. I retrieve

$$P_y = \frac{16ed}{9\pi^2}\begin{pmatrix} 0 & 0 & 0 \\ 0 & 0 & 1 \\ 0 & 1 & 0 \end{pmatrix} \qquad \text{and} \qquad P_z = \frac{16ed}{9\pi^2}\begin{pmatrix} 0 & 0 & 1 \\ 0 & 0 & 0 \\ 1 & 0 & 0 \end{pmatrix}. \tag{D3}$$

For the situation considered in this manuscript, the electric field $\mathcal{E}_z$ in the semiconducting wire is zero. Thus for only $\mathcal{E}_y$ finite, the channel $(1,2)$ decouples even in the presence of gauge potentials and the Hamiltonian for the two remaining coupled channels, $(2,1)$ and $(1,1)$, is identical to the two-channel film case of Sec. C. Note that the channel $(1,2)$ can not support Majorana fermions. If the proximity induced gap becomes z dependent, then it is possible for the $(1,1)$ and $(1,2)$ channels to couple. Nonetheless, even then the presence of the $(1,2)$ channel does not change the qualitative topological characteristics and only brings some quantitative modifications in the phase diagram. In order for this channel to become topologically relevant, a different type of spin-orbit coupling has to considered, which includes also the $\hat{p}_z$ momentum. As a matter of fact, only interchannel coupling induced by spin-orbit interaction, which will be converted into an effective Zeeman term, can lead to new topological properties due to the addition of the $(1,2)$ channel.

[1] G. Schön and A. D. Zaikin, *Quantum Coherent Effects, Phase Transitions and Dissipative Dynamics of Ultra Small Tunnel Junctions*, PHYSICS REPORTS (Review Section of Physics Letters) **198**, Nos. 5 & 6, 237-412 North-Holland (1990).

[2] T. D. Stanescu, J. D. Sau, R. M. Lutchyn, and S. Das Sarma, Phys. Rev. B **81**, 241310(R) (2010); A. C. Potter and P. A. Lee, Phys. Rev. B **83**, 184520 (2011).